Eur. Phys. J. B **5**, 67–77 (1998)

THE EUROPEAN PHYSICAL JOURNAL B

Structure and rheology of concentrated wormlike micelles at the shear-induced isotropic-to-nematic transition

J.-F. Berret[1,a], D.C. Roux[1,b] and P. Lindner[2]

[1] Unité Mixte de Recherche CNRS / Université de Montpellier II[c], Groupe de Dynamique des Phases Condensées, 34095 Montpellier Cedex 05, France,
[2] Institute Laue-Langevin, BP 156, 38042 Grenoble Cedex 9, France

Received: 16 February 1998 / Revised: 18 February 1998 / Accepted: 24 May 1998

Abstract. We have investigated the simple shear flow behavior of wormlike micelles using small-angle neutron scattering and mechanical measurements. Ternary surfactant solutions made of cetylpyridinium chloride, hexanol and brine (0.2 M NaCl) and hereafter abbreviated as CPCl-Hex were studied in the concentrated regime, $\phi \sim 30\%$. In a preliminary report (Berret *et al.* [16]), the discontinuity of slope observed in the shear stress *versus* shear rate curve was interpreted in terms of first-order phase transition between an isotropic state and a shear-induced nematic state (I−N transition). At the transition rate, $\dot{\gamma} = \dot{\gamma}_{\mathrm{I-N}}$, the solution exhibits a macroscopic phase separation into viscous and fluid layers (inhomogeneous shear flow). Above a second characteristic shear rate, the flow becomes homogeneous again, the sheared solution being nematic only. The neutron patterns obtained in the two-state inhomogeneous region have been re-examined. Based on a consistent analysis of both orientational and translational degrees of freedom related to the wormlike micelles, we emphasize new features for the I−N transition. In the present paper, the shear rate variations of the relative proportions of each phase in the two-state region, as well as the viscosity ratio between isotropic and nematic phases are derived. We demonstrate in addition that slightly above the transition rate, the shear induced nematic phase is already strongly oriented, with an order parameter $P_2 = 0.65$. The orientational state is that of a nematic flow-oriented monodomain. Finally, from the locations of the neutron scattering maxima for each isotropic and nematic contributions, we evaluate the concentrations for each phase ϕ_{I} and ϕ_{N} and derived a dynamical phase diagram of CPCl-Hex, in terms of the stress σ *versus* ϕ_{I} and ϕ_{N}. According to the classification by Schmitt *et al.* [22], the I−N transition observed in CPCl-Hex micellar solutions could result from a positive flow-concentration coupling, in agreement with the observed monotonically increasing shear stress in the two-phase region.

PACS. 61.30.Eb Experimental determinations of smectic, nematic, cholesteric, and other structures – 83.50.Gd Nonlinear viscoelasticity – 64.70.-p Specific phase transitions – 82.70.-y Disperse systems

1 Introduction

Wormlike micelles results from the self-assembling of surfactant molecules into a locally cylindrical and elongated aggregates. For these macromolecules, the contour lengths are supposed to greatly exceed a persistence length (~ 200 Å). Wormlike micellar solutions have stimulated considerable theoretical and experimental interests during the last years because of its unique and fascinating rheology [1,2].

In the late 80's, attention was paid to the linear viscoelasticity. In the linear response region, these complex fluids appear to be described by a simple Maxwell model. The low-frequency mechanical properties are determined by a plateau modulus G_0 and a unique relaxation time τ_R [3–10]. The plateau modulus G_0 characterizes the elasticity that can be stored by the network under strain, whereas τ_R describes the time scale of the relaxations occurring in a viscous dissipation process. One of the great success of the model imagined by Cates and coworkers [11,12] was to relate this terminal time τ_R to a double mechanism of relaxation in response to an externally applied strain. These authors took into account the reptation mechanism for relaxation of entanglements, combined with the reversible scission that the micellar chains experienced dynamically.

In the early 90's, it became obvious that the nonlinear mechanical properties are still more puzzling. Several experimental reports have emphasized the existence of a shear stress plateau observed in rate controlled experiments above a characteristic shear rate (*e.g.* [2]). Taking

[a] e-mail: `berret@gdpc.univ-montp2.fr`
[b] *Present address:* Pôle Européen de plasturgie, 2 rue Pierre et Marie Curie, 01100 Bellignat, France
[c] n° 5581

into account the reptation and reversible relaxations mentioned previously, Cates and coworkers [13,14] predicted a nonmonotonic constitutive equations for semi-dilute concentration range. The unstable part of the stress *versus* strain rate curve was replaced by a plateau in a so-called "top-jumping" scenario. It was assumed that as a result, the solution splits into two macroscopic layers of different fluidity, yielding an inhomogeneous stationary flow.

At the same time, experiments combining small-angle neutron scattering and rheology in concentrated solutions have proven that the discontinuity of slope in the $\sigma(\dot{\gamma})$-behavior evidenced a shear-induced transition between isotropic and nematic (I−N) phases [15,16]. Flow birefringence supported later on this picture since both phases organized into macroscopic layers perpendicular to the gradient direction could be directly observed [17,18]. Cates's constitutive equation [13] and its agreement with the data due to Rehage and Hoffman [2] on one side, and the evidence of a I−N first order transition on the other are in principle not contradictory since both are describing inhomogeneous shear flows in different concentration ranges. Other theoretical approaches than those mentioned above have attempted to model the effect of shear on dispersed systems of anisotropic species. In some cases these models yield a transition toward a nematic state [19–23].

Very recent rheological experiments on wormlike micelles however have revealed completely new and remarkable features. Grand *et al.* [24] have re-examined the steady-state nonlinear rheology of the well-known cetylpyridinium chloride / sodium salicylate solution first discovered by Rehage and Hoffman [2]. As in concentrated systems displaying a true shear-induced transition [9,25], these authors observed slow transient kinetics of the shear stress in the plateau regime, that they interpret in terms of metastability. These new measurements, as those of reference [26] on a parent solution, seem to rule out the top-jumping hypothesis originally postulated [13,14]. In order to account for the two-state banded flow and the slow transients of the band formation, Porte *et al.* [26] have proposed a phenomenological explanation for the inhomogeneous shear flow of wormlike micelles, provided that an effective non-equilibrium potential exists and obeys a variation principle. The transition is obtained by minimization of this potential, which considers the elastic free energy stored in the viscoelastic fluid under steady shear. Recent reports by Boltenhagen *et al.* [27] and Wheeler *et al.* [28] are showing that there exists wormlike micellar semidilute solutions that can first shearthinn and then exhibit a strong shearthickening effect. In Couette flows this thickening is concomitant to a macrophase separation of the sheared solution into turbid and transparent domains arranged either into layers [27] or into ring-like patterns stacked in the vorticity direction [28]. In the present paper, we re-examine the nonlinear rheology of concentrated wormlike micelles by combining small-angle neutron scattering (SANS) experiments under shear and mechanical measurements. The systems investigated here are the ternary solutions made of cetylpyridinium chloride, hexanol and brine (0.2 M NaCl) close to the isotropic-to-nematic phase boundary. In our preliminary letter [16] that will be referred to as (I) in the following, the effect of simple shear flow on wormlike micelles was analyzed in terms of a shear-induced phase transition between isotropic and nematic states. We will do the same here. A careful analysis of the neutron patterns in the two-state inhomogeneous region is presented in addition. Both orientational and translational degrees of freedom associated to the wormlike micelles in shearing fields are shown to be consistent, yielding a dynamical phase diagram and the evidence of a flow-concentration coupling for the CPCl-Hex system.

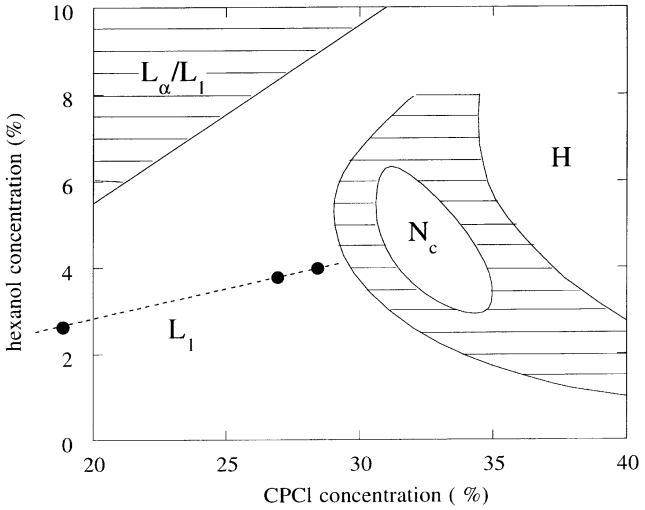

Fig. 1. (ϕ_{CPCl}, ϕ_{Hex})-phase diagram of the ternary surfactant system cetylpyridinium / hexanol / brine (0.2 M NaCl) in the low alcohol concentration range. For constant ratio R between hexanol and CPCl, the following sequence is observed on the dilution line: isotropic (L_1) / nematic calamitic (N_c) / hexagonal (H). L_α/ L_1 denotes a biphasic region where smectic and isotropic phases coexist. The concentrations of the phase boundaries for solutions prepared with water and deuterated water are compared in Table 1. The closed circles indicate the concentrations for which the shear stress is displayed in Figure 2. The dilution line $R = \phi_{\mathrm{Hex}}/\phi_{\mathrm{CPCl}} = 0.14$ is also shown (dotted line in the isotropic region).

2 Experimental details

2.1 Sample preparation and phase diagram

The cetylpyridinium chloride is obtained by Fluka and further purified by three recrystallisations, one in water and two in wet acetone ($T = 60\,^{\circ}\mathrm{C}$). Hexanol is also provided by Fluka but used with no further purification. For the preparation of the brine at 0.2 M NaCl, sodium chloride is obtained from Merck and used as received, while water was purified by passing a 4 filter Millipore 18 MΩ-water system. This preparation procedure [29,30] of the chemical species enables a excellent reproducibility of the static phase diagram. The static phase diagram of this

Table 1. List of the phase boundary concentrations for CPCl-Hex, using H_2O and D_2O as solvent. Both systems are along a dilution line fixed by the ratio between alcohol and surfactant ($R = 0.14$). Here, L_1 represents the disordered isotropic phase, N_c the nematic calamitic phase and H the hexagonal one.

CPCl-Hex $R = 0.14$	**biphasic** L_1- N_c	**nematic** N_c	**biphasic** N_c - H	**hexagonal** H
solvent H_2O	33.7%	35.4%	38.8%	40.8%
solvent D_2O	31.4%	33.0%	36.3%	38.3%

ternary surfactant system CPCl-Hex/H_2O (0.2 M NaCl) can be simplified, and described in terms of the concentration in alcohol *versus* that of surfactant. The original and complete (ϕ_{CPCl}, ϕ_{Hex})-phase diagram has been reported in the past [29]. We are here concerned with the low hexanol content ($\phi_{Hex} < 10\%$, see Fig. 1) and in the range where self-assembling results in locally cylindrical and elongated species. With increasing concentration, the different phases and mesophases in Figure 1 are the isotropic phase (L_1), the nematic calamitic phase (N_c) and hexagonal phase (H). This is the typical sequence which illustrates that packing of semi-flexible cylinders yields orientational (N_c, H) and then translational (H) orderings. We provide the phase boundary concentrations between L_1, N_c and H phases in Table 1, as determined for the two solvents H_2O and D_2O. The micellar solutions investigated here are made at constant ratio $R = \phi_{Hex}/\phi_{CPCl}$. When speaking in terms of total concentration ϕ, we always mean that the sum $\phi_{CPCl}+\phi_{Hex}$ has to be considered. This implicitly assumes that both cetylpyridinium and hexanol molecules are constituting the body of the cylindrical aggregates in a proportion which is unchanged when ϕ is increasing (*e.g.* on the dilution line $R = 0.14$ shown by a dotted line in Fig. 1). Neutron scattering on dilute as well as on concentrated hexagonal phases [30] confirmed this view. The radius of CPCl-Hex wormlike micelles is found to be remarkably constant, at $r_c = 21 \pm 1$ Å [30].

2.2 Rheology

The linear and nonlinear viscoelastic properties of the CPCl-Hex solutions were obtained on a Rheometrics Fluid Spectrometer using in a cone-and-plate (diameter 50, angle 0.02 radian) and a Couette (gap 1 mm) tool devices. Dynamical measurements ($T = 30\,°C$) were carried out for angular frequency $\omega = 0.1{-}100$ rad s^{-1}. This is a controlled shear-rate rheometer which is particularly well-suited to investigate this kind of shear-induced transition. For steady shear rate measurements (again $T = 30\,°C$), we focused on the stationary limits of the stress only. Long lasting transient responses which are typical features of the nonlinear rheology of wormlike micelles [9,25,26] will be detailed in a forthcoming publication on CPCl-Hex system [31]. Note finally that an anti-evaporation device was specially constructed for long-time measurements.

2.3 Small-Angle Neutron Scattering under shear

The SANS measurements were performed at the Orphée Reactor at the Laboratoire Léon Brillouin[1] on a CPCl-Hex solution at concentration $\phi = 31.07\%$. The alcohol and surfactant concentrations were $\phi_{Hex} = 3.33\%$ and $\phi_{CPCl} = 27.74\%$ respectively, corresponding to a mass ratio alcohol/surfactant of 0.12. D_2O was used as solvent in order to enhance the scattering contrast. This sample, though isotropic is very close to the biphasic isotropic/nematic boundary limit found with the deuterated solvent at $\phi = 31.4\%$ (with however $R = 0.12$, see Tab. 1). A 1 mm-gap neutron transparent Couette cell designed for elastic scattering was utilized as shearing device [32]. Due to flow instabilities at the air/solution interface, the upper accessible limit in strain rates was not more than 250 s^{-1}. For the measurements under steady shear, we used a radial scattering configuration. The incoming neutron beam (wave vector $\mathbf{k_i}$) passes through the cell normal to the rotation axis, *i.e.* with $\mathbf{k_i} \| \nabla\mathbf{v}$ and $\mathbf{k_i} \perp \mathbf{v}$. Scattering patterns are recorded on a two-dimensional XY detector (128×128 elements of 0.5×0.5 cm^2) located at 2 meters behind the sheared solutions, yielding the neutron intensity in the ($\mathbf{q_v}$, $\mathbf{q_e}$)-plane of the reciprocal space. Here, $\mathbf{q_v}$ and $\mathbf{q_e}$ are the wave-vectors parallel to the velocity $\mathbf{v}$ and vorticity $\mathbf{e} = \nabla\mathbf{v} \times \mathbf{v}$ directions in real space. Because of the relatively high surfactant concentration, there was a risk of multiple scattering. This was checked by using a 0.5 mm gap cell for which the final patterns were identical. At the wavelength of $\lambda = 6.29$ Å, the SANS experiments probed a q-range from 2×10^{-2} Å^{-1} to 1.7×10^{-1} Å^{-1}, with a resolution $\Delta q/q \sim 0.1$.

3 Results

3.1 Rheology

Wormlike micelles of CPCl-Hex are not very much viscoelastic. Except at the vicinity of the I–N transition, solutions prepared in the L_1-phase are all Newtonian [29,30]. For $\phi \leq \phi_{I-N}$, when static viscosities are in the range 1–10 Pa s, some viscoelasticity can be observed [16]. Typical relaxation times can be estimated from the behavior of the real and imaginary parts of the complex elastic modulus (not shown here). They are $\sim$ 10 ms, or even faster.

Figure 2 displays the steady state shear stress for three CPCl-Hex solutions at $\phi = 20.46\%$, 30.70% and $\phi = 32.40\%$ on a semilogarithmic plot. These samples are indicated by closed circles in the phase diagram of Figure 1. With increasing concentration the nonlinear response changes from purely Newtonian ($\phi = 20.40\%$, $\eta_0 = 0.63$ Pa s) to a behavior exhibiting two distinct flow regimes. For $\phi = 30.70\%$ and $\phi = 32.40\%$, at low strain rates, the fluid is again Newtonian, with static viscosities $\eta_0 = 6.1$ and 10.0 Pa s, respectively. At the characteristic strain rate $\dot{\gamma}_{I-N}$, the $\sigma(\dot{\gamma})$-curves exhibit a discontinuity

[1] The laboratoire Léon Brillouin is a "Laboratoire commun CEA-CNRS"

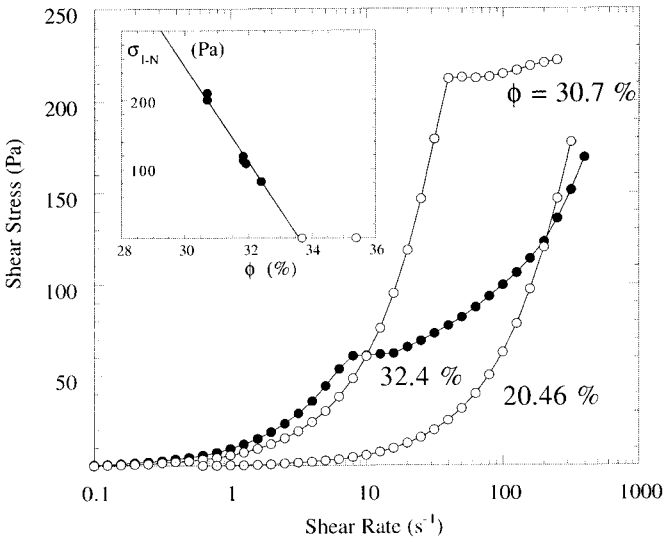

Fig. 2. Strain rate dependencies of the mechanical shear stress for three CPCl-Hex/H_2O solutions at $\phi = 20.46\%$, 30.70% and $\phi = 32.40\%$. Data are in steady state conditions. At low $\dot{\gamma}$, all fluids are Newtonian. For $\phi = 30.70\%$ and $\phi = 32.40\%$, the $\sigma(\dot{\gamma})$-data exhibit a discontinuity of slope toward a second flow regime at the characteristic strain rate $\dot{\gamma}_{I-N}$. This second region is referred to as a plateau or quasi-plateau regime. Inset: Concentration dependence of the transition shear stress $\sigma_{I-N} = \sigma(\dot{\gamma}_{I-N})$ for CPCl-Hex micellar systems close to the static isotropic-to-nematic transition. Note that $\sigma_{I-N}(\phi)$ extrapolates to zero shear stress at ϕ_{I-N}.

of slope toward a second flow regime ($\sigma > \sigma_{I-N}$). For the $\phi = 30.70\%$, a true stress plateau is revealed whereas for the $\phi = 32.40\%$ solution, the stress increases further beyond the cross-over. In this second regime, however, one can checked that the stress still increases according to a power law (actually not discernible on the semilogarithmic plot of Fig. 2). For $\phi = 32.40\%$ one gets $\sigma(\dot{\gamma}) \sim \dot{\gamma}^{0.26}$ whereas for the $\phi = 30.70\%$ solution, the exponent turns out to be 0.03. For this reason, we will refer to this second region as a plateau or quasi-plateau regime.

A solution was prepared with deuterated brine for the aim of neutron scattering at a total concentration $\phi = 31.07\%$. When submitted to steady shear, its nonlinear behavior is identical to the one described above [16]. Its rheological features at the transition Newtonian to pseudo-plateau regime (viscosity, transition rate and stress) are compared to those of CPCl-Hex/ H_2O (0.2 M NaCl) solutions in Table 2 (see Sect. 4.1. for additional details). In the inset of Figure 2, the concentration dependence of σ_{I-N} is displayed for the CPCl-Hex micellar system. Approaching the static Isotropic-to-Nematic transition concentration from below, $\sigma_{I-N}(\phi)$ decreases linearly with ϕ. It extrapolates remarkably to zero shear stress at ϕ_{I-N}. Note that the coexistence state for L_1 and N_c phases is found between $\phi_{I-N} = 33.7\%$ and $\phi = 35.4\%$ (open symbols in the inset).

Table 2. List of the viscoelastic parameters obtained for the surfactant ternary solutions CPCl-Hex at the transition between isotropic and nematic induced state. η_0 denotes the static viscosity, $\dot{\gamma}_{I-N}$ the transition strain rate, σ_{I-N} the value of the mechanical stress at the onset of the plateau regime. The last column displays the exponent for the scaling relation $\sigma(\dot{\gamma})$ in the coexistence region.

CPCl-Hex	η_0 (Pa s)	$\dot{\gamma}_{I-N}$ (s^{-1})	σ_{I-N} (Pa)	exponent
$\phi = 30.70\%$ (H_2O)	6.1	40 ± 1	212	0.03
$\phi = 32.40\%$ (H_2O)	10.0	8 ± 0.5	61	0.26
$\phi = 31.07\%$ (D_2O)	6.7	8 ± 1	46	0.29

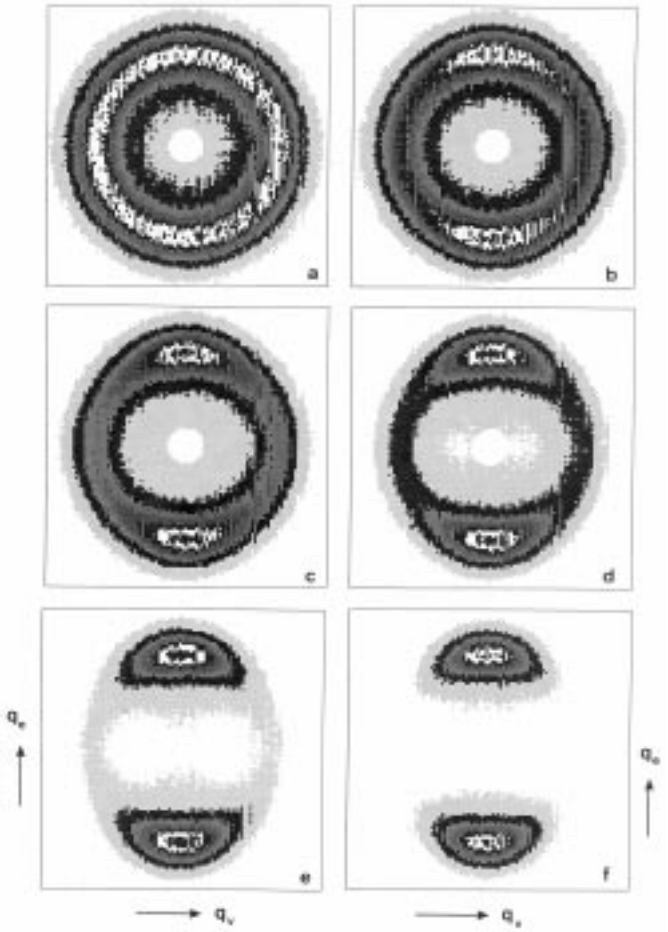

Fig. 3. Two dimensional neutron scattering patterns obtained for a CPCl-Hex solution prepared with deuterated solvent (D_2O, $\phi = 31.07\%$). Strain rates are $\dot{\gamma} = 0$ (Fig. 3a), 13 (3b), 32 (3c), 64 (3d), 128 (3e) and 213 s^{-1} (3f), respectively. The scattered neutron intensity is recorded in the ($\mathbf{q_v}$, $\mathbf{q_e}$)-plane of the reciprocal space ($\mathbf{q_v}$ horizontal axis, $\mathbf{q_e}$ vertical axis). Wave vectors in both $\mathbf{q_v}$ and $\mathbf{q_e}$-directions are between -0.16 $Å^{-1}$ and $+0.16$ $Å^{-1}$. The maximum scattering at $q^M = 0.0996$ $Å^{-1}$ attests of strong translational correlations between the micellar threads. Above $\dot{\gamma}_{I-N}$ ($= 8 \pm 1$ s^{-1}, Figs. 3b and following), the anisotropic scattering is due to a shear-flow-induced phase that has the orientational properties of a nematic phase.

3.2 Small-Angle Neutron Scattering

Figures 3a–3f show the two dimensional scattering patterns received from a CPCl-Hex solution prepared with deuterated solvent (D_2O, $\phi = 31.07\%$). Each spectrum corresponds to a different shear rate, which are $\dot{\gamma} = 0$ (Fig. 3a), 13 (3b), 32 (3c), 64 (3d), 128 (3e) and 213 s^{-1} (3f), respectively. The scattered neutron intensity is recorded in the ($\mathbf{q_v}$, $\mathbf{q_e}$)-plane of the reciprocal space, where $\mathbf{q_v}$ ands $\mathbf{q_e}$ are the abscise and ordinate axes. The full scale in both directions is for wave-vector comprised between -0.16 Å^{-1} and $+0.16$ Å^{-1}.

The rested solution exhibits a scattering ringlike pattern (Fig. 3a) characteristic of an isotropic concentrated micellar solution. The intensity is distributed isotropically independent on the directions in reciprocal space and has a broad maximum at $q^M = 0.0996$ Å^{-1}. This maximum attests of strong translational correlations between the micellar threads. A rough estimate of the distance separating collinear and neighboring center-of-mass yields $d = 2\pi/q^M = 63$ Å. With increasing $\dot{\gamma}$, anisotropy arises in the scattering. It manifests itself by the occurrence of symmetric crescent-like peaks in the $\mathbf{q_e}$-direction. Their location in transfer momentum at q_e^M is slightly changed with respect to the unsheared solution. This property will be discussed in detail in Section 4.2. Simultaneous to the growth of the anisotropic patterns, the ringlike structure vanishes progressively. It disappears seemingly at $\dot{\gamma} = 213$ s^{-1} (Fig. 3f). It should be emphasized that at higher shear rates (> 100 s^{-1}, Fig. 3d and 3e), the isotropic ring also shrinks to lower q-values. Starting from a fully circular pattern at rest, the overall scattering picture becomes oval-shaped. As documented in references [16,33,34], this pattern at $\dot{\gamma} = 213$ s^{-1} (Fig. 3f) is qualitatively analogous to the ones obtained from a surfactant solution that would be nematic at rest (*e.g.* $\phi > 33.0\%$, see Table 1) and subjected to a gentle shearing. This observation leaded us to interpret the discontinuity of slope in the $\sigma(\dot{\gamma})$-flow curve in terms of isotropic-to-nematic transition induced by shear [16]. We will do the same here, but will present a complete analysis of the scattering data. Of the utmost importance we will be able to relate consistently structural and mechanical results.

4 Analysis and discussion

The neutron and rheology data described above are now analyzed in terms of orientational and translational degrees of freedom. Orientational degrees of freedom refers to the angular distribution function of the micelles with respect to the flow velocity, and thus aims to describe the state of alignment of the shear-induced nematic phase. The translational degrees of freedom, on the other hand are related to the intermicellar mean distances in one or in the other phase, and thus reveal their respective volume fractions.

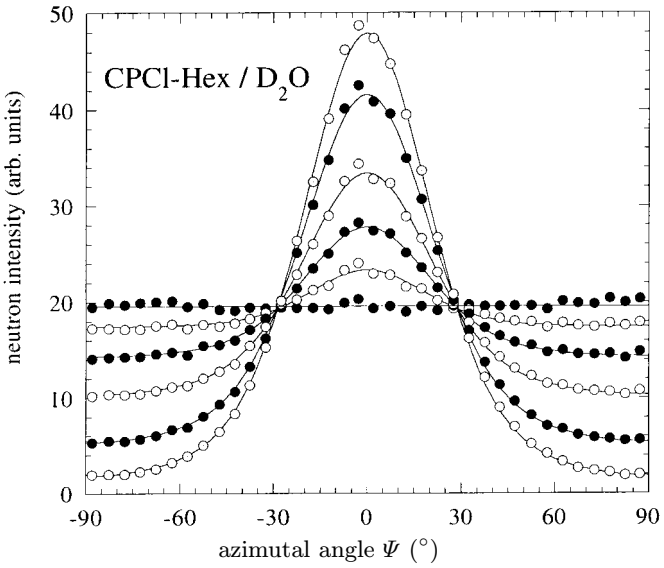

Fig. 4. Radially integrated intensity $I(q^M, \Psi)$ as function of the azimuthal angle Ψ for the $\phi = 31.07\%$ CPCl-Hex solution in deuterated solvent. Shear rates are $\dot{\gamma} = 0$, 13, 32, 64, 126 and 213 s^{-1} (the constant distribution corresponds to the rested solution). Here the anisotropy increases with the strain rate. Continuous lines results from best fit calculations using equation (1) which assumes two distinct contributions, one isotropic and one nematic.

4.1 Orientational degrees of freedom

For the first stage of the analysis of the neutron spectra, we follow the original approach of (I). The SANS spectra are analyzed in terms of angular distribution of the scattered intensity $I(q^M, \Psi)$. Here Ψ is the azimuthal angle that we defined as $\Psi = (q, q_e)$. Ψ is assumed to increase clockwise and is taken positive in the upper right quadrant. The neutron counts are integrated over the elementary surface $dq_v dq_e = q^M \Delta q^M \Delta\Psi$, where Δq^M corresponds to the half-width at half maximum of the scattering in both $\mathbf{q_v}$ and $\mathbf{q_e}$-directions ($\Delta q^M = 0.018$ Å^{-1} and $\Delta\Psi = 5°$). The resulting angular dependencies $I(q^M, \Psi)$ are displayed in Figure 4 for different shear rates $\dot{\gamma} = 0, 13, 32, 64, 126$ and 213 s^{-1}). As expected, this azimuthal distribution is constant in the isotropic phase, and as far as the sheared solution enters the two-phase domain, a periodic function is obtained with maxima in the $\mathbf{q_e}$-directions, for $\Psi = 0°$ and 180° (only data for $\Psi = -90°$ to $\Psi = 90°$ are shown in Fig. 4).

The $I(q^M, \Psi)$-function illustrated in Figure 4 is indicative of the local angular distribution of the surfactant aggregates since it is computed at a wave vector corresponding to the first maximum in the structure factor. In (I), the orientational distribution of scattering intensity was interpreted as the sum of two components, one purely isotropic (thus constant in the representation of Fig. 4) and one anisotropic over the whole $\dot{\gamma}$-range. In the plateau regime, these contributions were said to originate from two different phases that have separated macroscopically: one isotropic and one nematic phase. From neutron scattering

solely, such a conclusion cannot be rigorously deduced. Actually, the growing anisotropy revealed in Figure 4 could be interpreted as well, in terms of a progressive alignment of the micellar threads. The crucial experiment on wormlike micelles under shear has been the *in situ* birefringence measurements with the polarized light propagating along the vorticity direction of a Couette cell [17,19,35]. These experiments demonstrated unambiguously the coexistence of two-phase of different birefringence, viscosity and order parameter. Concentrated CPCl-Hex solutions have been tested using this powerful technique and were found to exhibit coexisting phases above $\dot{\gamma}_{\mathrm{I-N}}$ [36]. Considering the above arguments, we now can express the azimuthal intensity $I\,(q^M,\,\Psi)$ as:

$$I\,(q^M,\,\Psi,\,\dot{\gamma}) = I_{\mathrm{I}}(\dot{\gamma}) + I_{\mathrm{N}}(\Psi,\,\dot{\gamma})$$
$$\text{with}\quad I_{\mathrm{N}}(\Psi,\,\dot{\gamma}) = I^0_{\mathrm{N}}(\dot{\gamma})\sinh(b\cos^2\Psi). \qquad (1)$$

Here, $I_{\mathrm{I}}(\dot{\gamma})$ denotes the Ψ-independent contribution of the isotropic phase, $I^0_{\mathrm{N}}(\dot{\gamma})$ the prefactor to the nematic component. The Ψ-dependence of $I_{\mathrm{N}}(\Psi,\,\dot{\gamma})$ is taken to be periodic, and characterized by a unique factor b, which determines the order parameter of the oriented phase. This analytical expression is slightly different from the one used in (I). Equation (1) assumes that the shear-induced nematic phase scatters only in the vorticity direction (this was not the case for the approximate function of (I)). Best fit calculations using equation (1) are shown in Figure 4 as continuous lines, where $I_{\mathrm{I}}(\dot{\gamma})$, $I^0_{\mathrm{N}}(\dot{\gamma})$ and b have been treated as adjustable parameters.

Considering the above set of data related to the orientational degrees of freedom in the two-phase domain, we will now distinguish three sub-sections: 4.1.1 evolution of the proportions of each phase in the quasi-plateau regime, 4.1.2 calculation of the order parameter of the shear-induced nematic phase and 4.1.3 the derivation of the ratio of the viscosities of each phase using a relationship between structure and rheology.

4.1.1 Evolution of the proportions of isotropic and nematic phases in the quasi-plateau regime

The relative proportions of each phase in the two-phase domain ($\dot{\gamma} > \dot{\gamma}_{\mathrm{I-N}}$) are easily determined from the fitting procedure previously mentioned. They are $\varepsilon_{\mathrm{I}}(\dot{\gamma}) = I_{\mathrm{I}}(\dot{\gamma})/I_{\mathrm{T}}(\dot{\gamma})$ and $\varepsilon_{\mathrm{N}}(\dot{\gamma}) = (1/I_{\mathrm{T}}(\dot{\gamma}))\int_0^{2\pi} I_{\mathrm{N}}(\Psi,\,\dot{\gamma})d\Psi$ where $I_{\mathrm{T}}(\dot{\gamma})$ is the total scattered intensity calculated at each strain rate. $\varepsilon_{\mathrm{I}}(\dot{\gamma})$ and $\varepsilon_{\mathrm{N}}(\dot{\gamma})$ are displayed in Figure 5b as function of $\dot{\gamma}$ and have been checked to verify $\varepsilon_{\mathrm{I}}(\dot{\gamma}) + \varepsilon_{\mathrm{N}}(\dot{\gamma}) = 1$. Figure 5 indicates that the biphasic range is rather broad, since it extends from $\dot{\gamma} = 8\ \mathrm{s}^{-1}$ to $\sim 300\ \mathrm{s}^{-1}$. Actually, at the higher strain rate accessible with the neutron cell (Fig. 3), $\dot{\gamma} = 213\ \mathrm{s}^{-1}$), nearly 10% of the initial phase is still present. Such large quasi-plateau regime have been already reported for wormlike micelles undergoing shear-induced transition (CPCl/Sal [9], CTAB [17,35] *etc.*). In order to facilitate the comparison between rheological and structural data, the original results for stress and viscosity obtained on CPCl-Hex/ D_2O ($\phi = 31.07\%$) are shown in Figure 5a (see also (I)). The discontinuity of slope in the $\sigma(\dot{\gamma})$-behaviour associated with shear-thinning coincides well with the onset of anisotropy in SANS ($\varepsilon_{\mathrm{N}}(\dot{\gamma}) \neq 0$).

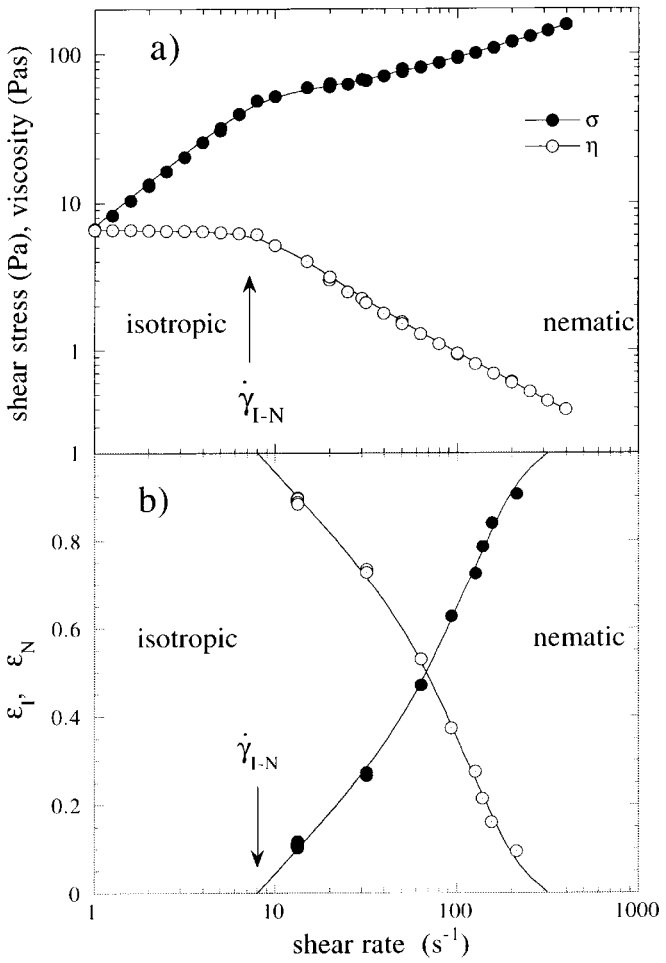

Fig. 5. (a) Variation of the steady shear stress and viscosity $\sigma(\dot{\gamma})$ and $\eta(\dot{\gamma}) = \sigma(\dot{\gamma})/\dot{\gamma}$ respectively for the CPCl-Hex/D_2O solution ($\phi = 31.07\%$) investigated by SANS. (b) Shear rate dependencies of the relative proportions of each phase ($\varepsilon_{\mathrm{I}}(\dot{\gamma})$ for isotropic, $\varepsilon_{\mathrm{N}}(\dot{\gamma})$ for nematic) in the two-phase domain. $\varepsilon_{\mathrm{I}}(\dot{\gamma})$ and $\varepsilon_{\mathrm{N}}(\dot{\gamma})$ are determined from the azimuthal distribution displayed in Figure 4, according to the procedure explained in the text. For this solution, the biphasic range extends from $\dot{\gamma} = 8\ \mathrm{s}^{-1}$ to $\sim 300\ \mathrm{s}^{-1}$. Note that the discontinuity of slope in the $\sigma(\dot{\gamma})$-behaviour in part (a) of the figure coincide well with the appearance of the anisotropic neutron scattering seen in part (b) The continuous lines are guides for the eyes.

4.1.2 Order parameter of the shear-induced nematic phase

The degree of orientation of the shear-induced nematic phase can be characterized quantitatively in terms of (local) order parameter P_2. P_2 is the second-order moment of the orientational distribution function, also defined as the average of $1/2\left(3\cos^2\beta - 1\right)$ over all orientations, where

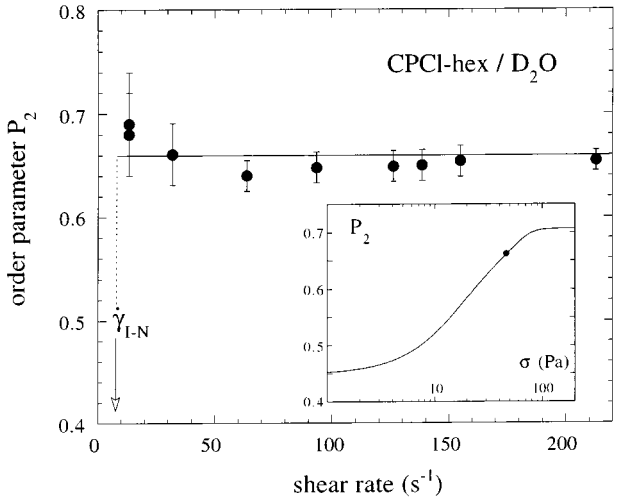

Fig. 6. Variation of the nematic order parameter P_2 as function of the shear rate in the quasi- plateau regime for the shear-induced phase (CPCl-Hex, $\phi = 31.07\%$). Its orientation state remains unchanged at $P_2 = 0.65 \pm 0.03$ in the two-phase region. Inset: the order parameter as determined from equation (2) for a nematic phase at $\phi = 35.25\%$ as function of the shear stress [33]. This $P_2(\sigma)$-behavior emphasizes that once created, the new phase is in a state of orientation comparable to that of a shear-oriented monodomain evidenced in the liquid-crystalline counterpart.

β is the angle made by a micellar thread with respect to the flow velocity. Analytical expressions were obtained recently by Deutsch [37], using a technique which enables to derive nth-order moment of the orientational distribution function directly from the scattering intensity $I_{\rm N}(\Psi, \dot\gamma)$. As provided in reference [37], P_2 reads:

$$P_2 = 1 - \frac{3}{2Z}\int_0^{\pi/2} I_{\rm N}(\Psi, \dot\gamma) \times \left[\sin^2\Psi + \sin\Psi\cos^2\Psi \ln\left(\frac{1+\sin\Psi}{\cos\Psi}\right)\right] d\Psi \quad (2)$$

where $Z = \int_0^{\pi/2} I_{\rm N}(\Psi) d\Psi$. Contrary to what has been claimed in recent reports [38], equation (2) provided reliable results, especially on the Maier-Saupe distribution function for which the order parameters are tabulated and known. P_2-data of the shear-induced nematic phase are shown in Figure 6 as function of the shear rate. Within the experimental accuracy, $P_2(\dot\gamma)$ remains constant in the quasi-plateau regime at $P_2 = 0.65 \pm 0.03$. Figure 5 indicates that the orientational distribution function of the aggregates with respect to the flow is not affected by the increasing rate. Similar conclusions were drawn in (I), though no estimation of the order parameters was made.

In (I), the constancy of the distribution function in the quasi-plateau regime was argued to be a strong indication of a first-order phase transition that is induced by shear. Two phases of different orientational order parameters were coexisting above $\dot\gamma_{\rm I-N}$. And thus, the shear rate was just the control parameter that adjusts the proportion of each phase (as the volume does it in the liquid-gas transition). Such a conclusion is actually valid for true stress plateau, *i.e.* $\sigma(\dot\gamma) = \sigma_{\rm I-N}\dot\gamma^0$. True stress plateaus have been observed in several viscoelastic surfactants, *e.g.* CPCl-NaSal [2,9,24,25], CTAB [35] *etc.*, but not in the CPCl-Hex solutions we are studying. As shown in Table 2 and in Figure 5, the stress continues to increase in the quasi-plateau region. And so should be the state of orientation of the nucleated nematic phase.

The apparent contradiction between a stress that scales with $\sigma \sim \dot\gamma^{0.29}$ (we are dealing with the deuterated solution) and a constant P_2 can be solved, taking into account the data recently reported on the liquid-crystalline mesophase of CPCl-Hex (in a nematic state at $\phi = 35.25\%$) [33]. The shear flow properties of nematic wormlike micelles are complex, and their study is out of the scope of the present paper. In reference [33], it was shown that the order parameter of nematic wormlike micelles increases with shear rate, starting in the texture region at $P_2 = 0.45$ ($\dot\gamma < 1$ s^{-1}) and leveling off in the monodomain region around $P_2 = 0.7$ ($\dot\gamma > 50$ s^{-1}). Here, we assume that the nematic phases of wormlike micelles induced by increasing either shearing or concentration are similar [16,33,34]. In the inset of Figure 6 we have reconstructed the evolution of the order parameter as function of the shear stress for the nematic solution at $\phi = 35.25\%$. Note that in [33], measurements of both shear stress and order parameter were originally performed *versus* strain rates. For the shear-induced I−N transition, the shear stress $\sigma_{\rm I-N}$ at the onset of quasi-plateau regime is 46 Pa (indicated in the inset of Fig. 6). This relatively high value of the stress corresponds, for the liquid-crystalline counterpart, to a nearly oriented nematic monodomain with an order parameter $P_2 = 0.66$. The agreement between this latter value and that of the order parameter of the shear-induced nematic phase ($P_2 = 0.65 \pm 0.03$, Fig. 6) is excellent. We can then conclude that in the coexisting region of the I−N transition, the nematic induced-phase is already strongly oriented. These findings justify *a posteriori* the approach in terms of orientational order parameter given by equation (2), since this latter equation is not valid for textural materials. Moreover, the hypothesis of shear-induced tumbling can be excluded [34]. In conclusion, we are able to explain why the orientational distribution (and so P_2) does not change noticeably while $\sigma(\dot\gamma)$ does.

4.1.3 Ratio of the isotropic and nematic viscosities as deduced from a relationship between orientational order and rheology

As revealed by flow birefringence experiments in the quasi-plateau regime [17,18,35], macroscopic layers of isotropic and nematic wormlike micelles coexist. Let us denote $\eta_{\rm I}$ and $\eta_{\rm N}$ their respective viscosities. For $\dot\gamma > \dot\gamma_{\rm I-N}$ and $\sigma > \sigma_{\rm I-N}$, two conservation laws can be postulated. In a controlled strain rate experiment where a macroscopic rate $\dot\gamma$ is applied to the solution, the shear stress is a continuous variable along the gradient direction, and thus identical in

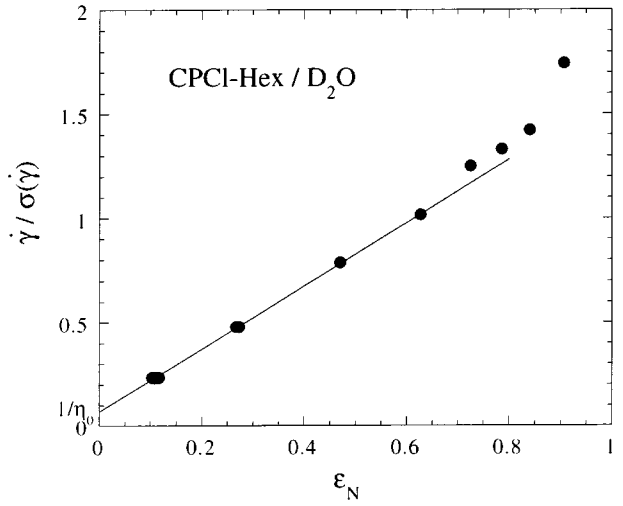

Fig. 7. Comparison between results obtained from the structure and from the rheology of CPCl-Hex solution in the two-phase region. The ratio $\dot{\gamma}/\sigma(\dot{\gamma})$ deduced from the flow curve (as in Fig. 2) is plotted *versus* the proportion of nematic induced phase $\varepsilon_{\rm N}(\dot{\gamma})$ (shown in Fig. 5). According to equation (5), the straight line enables to estimate the viscosity ratio $\alpha = \eta_{\rm I}/\eta_{\rm N}$ between the isotropic and nematic phases. We found $\alpha \sim 10{-}20$, depending on the constraint imposed at $\varepsilon_{\rm N}(\dot{\gamma}) \to 0$ (see text).

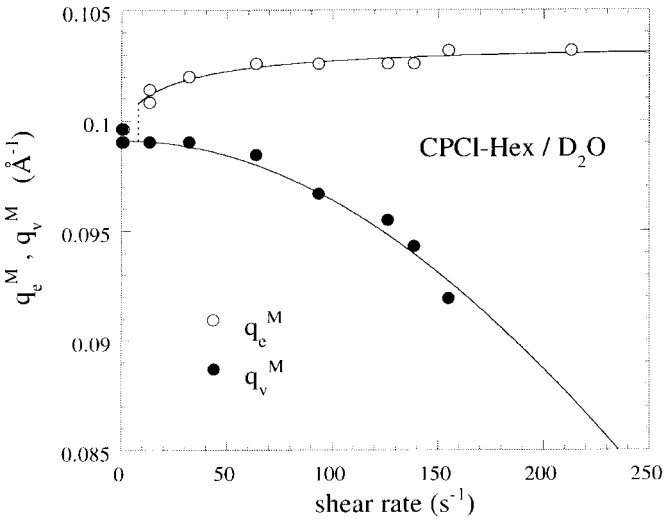

Fig. 8. Wave-vectors $q_{\rm v}^M$ and $q_{\rm e}^M$ at the maximum neutron intensity observed in the velocity and vorticity directions respectively for CPCl-Hex/ D_2O ($\phi = 31.07\%$). Above $\dot{\gamma}_{\rm I-N}$, the maximum wave-vectors split into two distinct behaviors: $q_{\rm e}^M$ rises to an almost constant value around 0.102 Å^{-1} whereas $q_{\rm v}^M$ decreases by about 10%. The continuous lines are guides for the eyes.

each phase:

$$\sigma(\dot{\gamma}) = \eta_{\rm I}\dot{\gamma}_{\rm I} = \eta_{\rm N}\dot{\gamma}_{\rm N} \tag{3}$$

where $\dot{\gamma}_{\rm I}$ and $\dot{\gamma}_{\rm N}$ are the strain rates experienced by the disordered isotropic and oriented nematic phase, respectively. Both $\dot{\gamma}_{\rm I}$ and $\dot{\gamma}_{\rm N}$ have first to obey the constraint imposed by the macroscopic rate, but also depends on the relative amount of each phase through the relation:

$$\dot{\gamma} = \varepsilon_{\rm I}(\dot{\gamma})\dot{\gamma}_{\rm I} + \varepsilon_{\rm N}(\dot{\gamma})\dot{\gamma}_{\rm N}. \tag{4}$$

Contrary to references [9,25] where attention was paid to the transient rheology, we focus here on the stationary state of shearing. Removing $\dot{\gamma}_{\rm I}$ and $\dot{\gamma}_{\rm N}$ from equations (3) and (4) yields a linear expression of the ratio $\dot{\gamma}/\sigma(\dot{\gamma})$ *versus* $\varepsilon_{\rm N}(\dot{\gamma})$:

$$\frac{\dot{\gamma}}{\sigma(\dot{\gamma})} = \frac{1}{\eta_{\rm I}}\left(1 + (\alpha - 1)\,\varepsilon_{\rm N}(\dot{\gamma})\right). \tag{5}$$

It should be noticed that since the stress is still increasing in the biphasic state, both viscosities $\eta_{\rm I}$ and $\eta_{\rm N}$, and so, their ratio α are in principle depending on the macroscopic applied rate. Equation 5 enables to compare data received from rheology and neutron scattering, namely the measured shear stress for a given applied rate and the proportion of nematic phase, respectively. This comparison is provided in Figure 7 for CPCl-Hex at $\phi = 31.07\%$. The straight line in Figure 7 emphasizes the linearity of $\dot{\gamma}/\sigma(\dot{\gamma})$ *versus* $\varepsilon_{\rm N}(\dot{\gamma})$ over a rather wide $\dot{\gamma}$-range (up to $\sim 100\ \text{s}^{-1}$). The fitting parameters are the viscosity of the isotropic phase at $\dot{\gamma}_{\rm I-N}$, $\eta_{\rm I}\,(\dot{\gamma}_{\rm I-N}) = 14$ Pa s), and the viscosity ratio $\alpha = 23$. The extrapolated value of $\dot{\gamma}/\sigma(\dot{\gamma})$ at $\varepsilon_{\rm N}(\dot{\gamma}) = 0$ is slightly lower than the inverse static viscosity of the rested solution ($\eta_0 = 6.7$ Pa s, see Tab. 2). When on the contrary we force the ordinate at origin to be $1/\eta_0$, the adjustments of equation (4) to the neutron data is less impressive than in Figure 7, and the viscosity ratio is lowered to $\alpha = 10$. The main result of Figure 7 is that the viscosity of the nematic phase is $\sim 10{-}20$ times lower than the one of the isotropic phase. Such values are in qualitatively agreement with the estimations based on the respective flow curves of isotropic and nematic phases. Related to the linearity observed in Figure 7, one can also conclude that even if the viscosities of each phase are (most likely) varying with strain rate, their ratio α is constant up to $\sim 100\ \text{s}^{-1}$. We have no explanation for this phenomenon.

4.2 Translational degrees of freedom

We now turn to the shear rate evolution of the position in wave vectors of each contribution. From Figure 3, we have seen that the isotropic ring-like pattern shrinks to lower wave-vectors when the shear rate is increased. In the two-phase region, the maximum scattering of the isotropic phase is assumed to be at best determined in the $\mathbf{q_v}$-direction, at a wave-vector defined by $q_{\rm v}^M$. The nematic crescent patterns have a maximum in the perpendicular direction at $q_{\rm e}^M$. $q_{\rm v}^M$ and $q_{\rm e}^M$ are displayed in Figure 8 in the whole $\dot{\gamma}$-range. Above $\dot{\gamma}_{\rm I-N}$, the maximum wave-vectors split into two distinct behaviors: $q_{\rm e}^M$ rises to an almost constant value, around 0.102 Å^{-1}, and $q_{\rm v}^M$ decreases by about 10%. These behaviors can be interpreted in terms of variations of the volume fraction of wormlike micelles in

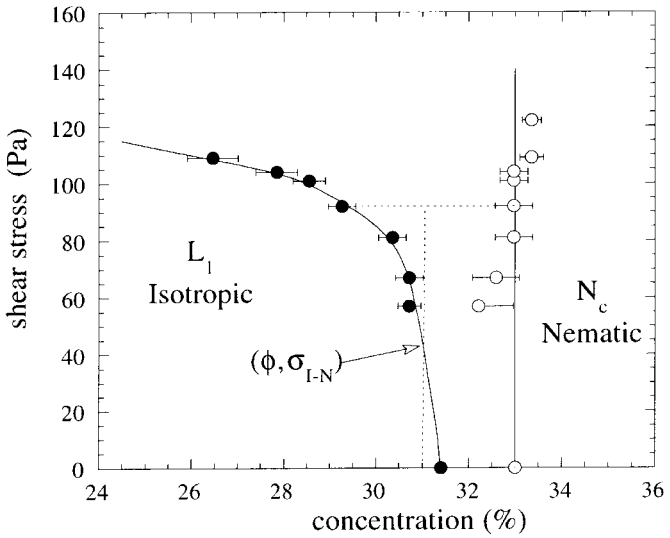

Fig. 9. Dynamical phase diagram (σ, $\phi_{\mathrm{I-N}}$) deduced from the comparison between structure and rheology measurements on CPCl-Hex wormlike micelles. The concentrations ϕ_{I} and ϕ_{N} of the two phases in the coexisting range are related to the positions of these scattering maxima through equation (6) (see Fig. 8). The concentration of the nematic phase stabilizes rapidly at $\phi_{\mathrm{I-N}} = 0.33$, which is the first concentration of a fully nematic solution at rest (in the D_2O-phase diagram). The remaining isotropic phase dilutes progressively as its proportion vanishes.

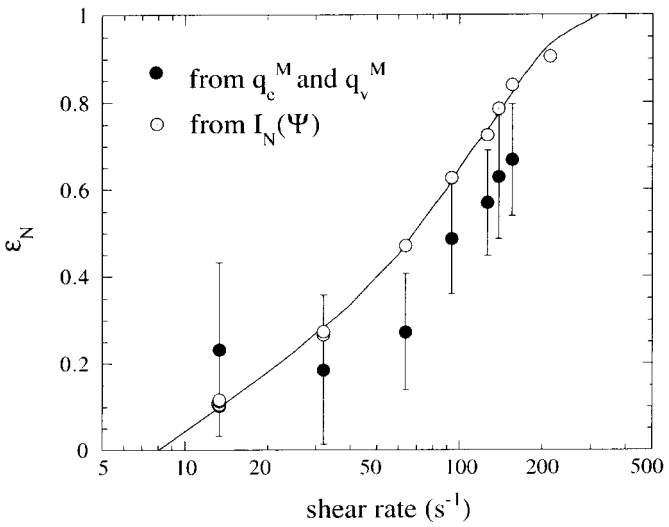

Fig. 10. Comparison of the nematic proportion $\varepsilon_{\mathrm{N}}(\dot{\gamma})$ determined from the analysis of the neutron patterns in terms distribution of micellar orientations (open symbols) and from the dynamical phase diagram (σ, $\phi_{\mathrm{I-N}}$) *via* the lever rule (Eq. (7), closed symbols). The continuous line is a guide for the eyes.

each phase. Actually, assuming a locally hexagonal packed arrangement of the cylindrical micelles, the concentrations ϕ_{I} and ϕ_{N} are related to the positions of these maxima through the expression:

$$\phi_{\mathrm{I,N}} = \frac{r_c^2\sqrt{3}}{8\pi}\left(q_{\mathrm{v,e}}^M\right)^2 \qquad (6)$$

where r_c is the radius of the micelles (we suppose the density of the fluid to be 1). In the homogeneous flow regime, where $q^M = 0.0996$ Å^{-1} and $\phi = 0.3107$, equation (6) yields a value for the micellar radius $r_c = 21.3$ Å, in good agreement with earlier reports [30]. According to equation (6), the variations of q_{e}^M and q_{v}^M observed in Figure 8 indicate first that the concentration of the nematic phase is slightly higher than that of the isotropic phase. Actually, and within the error bars, it stabilizes very soon at $\phi = \phi_{\mathrm{I-N}} = 0.33$, which we recall is the first concentration of a fully nematic solution at rest (in the D_2O-phase diagram, see Tab. 1). On the other hand, the remaining isotropic phase dilutes progressively as its proportion vanishes. This enables us to draw in Figure 9 a dynamical phase diagram of CPCl-Hex. There, the mechanical shear stress deduced from the flow curve is plotted against both concentrations ϕ_{I} and ϕ_{N} computed using equation (6). This diagram is strongly reminiscent to the schematical one in our first report (Fig. 5 in (I)). However, it is now based on concentrations calculated directly from the neutron data.

Figure 9 can be read as follows. With increasing shear rate, the stress first grows linearly. At $\sigma = \sigma_{\mathrm{I-N}}$ (indicated by an arrow in Fig. 9), the sheared solution enters the two-phase domain. The shear-induced nematic phase adopts at once the concentration corresponding to that of a nematic state at rest. In order to compensate both increases in ϕ_{N} and ε_{N}, the disordered phase lowers its concentration progressively. Because of the $\phi_{\mathrm{I,\ N}}(\dot{\gamma})$-variations above $\sigma_{\mathrm{I-N}}$, the shear stress continues to increase in the two-phase region. A true σ-plateau on the contrary would have indicated that the oriented induced phase has a concentration necessarily identical to the remaining isotropic one. We thus suggest that a quasi-plateau behavior in the flow curve of wormlike micelles is the signature of a coupling between concentration and shearing field.

For a stress in the biphasic region ($\sigma > \sigma_{\mathrm{I-N}}$), the lever rule should apply as for equilibrium first-order phase transition and the proportion of each phase can be again determined. One has for instance,

$$\varepsilon_{\mathrm{N}}(\dot{\gamma}) = \frac{\phi - \phi_{\mathrm{I}}(\dot{\gamma})}{\phi_{\mathrm{N}}(\dot{\gamma}) - \phi_{\mathrm{I}}(\dot{\gamma})}\cdot \qquad (7)$$

Figure 10 proposed a comparison of the nematic proportion determined with two methods. One set of data results from the analysis in terms distribution of micellar orientations (the same as in Fig. 5), the second set of data stems from the dynamical phase diagram of Figure 9 (*i.e.* using Eq. (7)). Despite a quite large uncertainty for the latter data, the agreement is qualitative. The difference could be due to an overestimation of the nematic proportion derived from the orientational distribution [35]. The assumption which consisted to assert that the anisotropic scattering results uniquely from the nematic phase is probably too restrictive. At high shear rates, one could also imagine that the more viscous phase exhibits some anisotropy (observed *e.g.* by means of birefringence) which in the spirit of equation (1) will not be taken into account.

5 Concluding remarks

Results of Figure 10 enable us to draw a self consistent picture of the I−N transition in CPCl-Hex surfactant wormlike micelles. The careful analysis of the neutron data performed separately in terms of orientational and translational degrees of freedom provides a unique scenario of the transition. For that micellar system, there exists a coupling between the velocity gradient (or velocity field itself) and the volume fraction of micelles. When sheared from a state at rest above $\dot{\gamma}_{\mathrm{I-N}}$, the solution exhibits a macroscopic phase separation into viscous and fluid layers. This separation is accompanied by the diffusion of the surfactant molecules from the more viscous to the more fluid phase. Such a transition driven by a coupling between the concentration and the flow characteristics has been treated theoretically by Schmitt *et al.* [22] and by Olmsted and Lu [23]. According to the classification by the first authors [22], the I−N transition detected in CPCl-Hex micellar solution is due to a positive flow-concentration coupling. Concentration fluctuations induce shear stress fluctuations, which in feedback generate an amplification of the concentration fluctuations. Finally the flow becomes inhomogeneous. Sloped plateaus and discontinuous flow curves related to a shear induced I−N transition have been found by Olmsted and Lu [23] in concentrated solutions of rod-like molecules. Of particular interest are the dynamic phase diagrams in the planes (σ, ϕ) and ($\dot{\gamma}$, ϕ) proposed by these authors. The coexistence state of disordered and nematic rod phases in shear flow is associated to a unique path (tie line in [23]) between the low and high strain rate stable branches through a selection criterion. This selection criterion is not postulated but is contained in the full inhomogeneous equations of motions. More convincingly, reference [23] demonstrates explicitly that due to the coupling mentioned above, the plateau is steeper close to the I−N transition and shallower farther away (see Fig. 2).

Compared to the first report on the I−N transition which together with reference [15] recognized the relevance of a combined analysis of structural and mechanical results, the present paper emphasizes new insights. They are:

(i) The shear rate dependencies of the relative proportions of each phase in the two-phase region were derived.

(ii) At the onset of the transition, the shear induced nematic phase is already strongly oriented (order parameter $P_2 = 0.66$). The orientational state is that of a nematic monodomain, analogous to what was found for nematic mesophases of wormlike micelles subjected to strain rates higher than 50 s^{-1} (with no or few textures and defects created by the flow) [33]. Having established that the shear-induced state is highly oriented, we have solved the apparent contradiction between a constant order parameter in the two-phase region and an increasing stress in the quasi-plateau regime.

(iii) Combining rheological data of the shear stress with the proportions of the nucleated nematics received from SANS, we have estimated the viscosity ratio of the coexisting phases, $\alpha = \eta_{\mathrm{I}}/\eta_{\mathrm{N}} \sim 10-20$.

(iv) A dynamical phase diagram intends to provide a representation of the phase behavior as function of the state of shearing. The mechanical shear stress was used as a new ordinate axis to describe a given state of shearing. From the SANS patterns, we have been able to evaluate the respective concentrations of each phase at every $\dot{\gamma}$ in the two-phase region. And thus, a purely experimental phase diagram under shear for these of wormlike micelles has been proposed (Fig. 9). Besides this analysis in terms of dynamical phase diagram, we also evidence a direct coupling between flow and concentration.

The authors would like to acknowledge numerous and fruitful discussions with G. Porte, M.E. Cates, J. L. Harden and P. Olmsted. We thank also A. Brûlet from then Laboratoire Léon Brillouin for her assistance during the experiments and her help in the analysis of the neutron data. The present work is partly founded by the European Community, through the European Network "Rheology of Liquid Crystalline Materials" (contract N° FMRX-CT96-0003 (DG 12-ORGS). During the course of this work, we have benefited from a stimulating environment provided by the GDR 1081 "Rhéophysique des colloïdes et suspensions" financed by the Centre National de la Recherche Scientifique.

References

1. M.E. Cates, S.J. Candau, J. Phys. Condens. Matter **2**, 6869 (1990).
2. H. Rehage, H. Hoffmann, Mol. Phys. **74**, 933 (1991).
3. H. Thurn, M. Löbl, H. Hoffmann, J. Phys. Chem. **89**, 517 (1985); H. Rehage, H. Hoffmann, J. Phys. Chem. **92**, 4712 (1988);
4. T. Shikata, H. Hirata, E. Takatori, T. Kotaka, Langmuir **3**, 1081 (1987); T. Shikata, H. Hirata, E. Takatori, K. Osaki, J. Non-Newt. Fluid Mech. **28**, 171 (1988).
5. P. Shurtenberger, R. Scartazzini, P.L. Luisi, Rheol. Acta **28**, 372 (1989).
6. F. Kern, R. Zana, S.J. Candau, Langmuir **7**, 1344 (1991); A. Khatory, F. Lequeux, F. Kern, S.J. Candau, Langmuir **9**, 1456 (1993).
7. P. Terech, V. Schaffhauser, P. Maldivi, J.M. Guenet, Langmuir **8**, 2104 (1992).
8. T.M. Clausen, P.K. Vinson, J.R. Minter, H.T. Davis, Y. Talmon, W.G. Miller, J. Phys. Chem. **96**, 474 (1992).
9. J.-F. Berret, J. Appell, G. Porte, Langmuir **9**, 2851 (1993); J.-F. Berret, D.C. Roux, G. Porte, J. Phys. II France **4**, 1261 (1994).
10. J.F.A. Soltero, J.E. Puig, O. Manero, Langmuir **12**, 2654 (1995).
11. M.E. Cates, Macromol. **20**, 2289 (1987); Idem, J. Phys. **49**, 1593 (1988).
12. R. Granek, M.E. Cates, J. Chem. Phys. **96**, 4758 (1992).
13. N.A. Spenley, M.E. Cates, T.C.B. MacLeish, Phys. Rev. Lett. **71**, 939 (1993).
14. N.A. Spenley, X.F. Yuan, M.E. Cates, J. Phys. II France **6**, 551 (1996); P.T. Callaghan, M.E. Cates, C.J. Rofe, J.B.A.F.H Smeulders, J. Phys. II France **6**, 375-393 (1996).

15. V. Schmitt, F. Lequeux, A. Pousse, D. Roux, Langmuir **10**, 955 (1994).
16. J.-F. Berret, D.C. Roux, G. Porte, P. Lindner, Europhys. Lett. **25**, 521 (1994).
17. E. Cappelaere, R. Cressely, J.-P. Decruppe, Coll. Surf. **104**, 353-374 (1995).
18. R. Makhloufi, J.-P. Decruppe, A. Aït-Ali, R. Cressely, Europhys. Lett. **32**, 253-258 (1995).
19. S. Hess, Z. Naturforsch. **31a**, 1507 (1976).
20. H. See, M. Doi, R. Larson, J. Chem. Phys. **92**, 792 (1990).
21. P. Olmsted, P. Goldbart, Phys. Rev. A **46**, 4966 (1992).
22. V. Schmitt, C. Marques, F. Lequeux, Phys. Rev E **52**, 4009 (1995).
23. P.D. Olmsted, C.-Y. D. Lu, Phys. Rev. E **56**, R55-R58 (1997).
24. C. Grand, J. Arrault, M.E. Cates, J. Phys. II France **7**, 1071-1086 (1997).
25. J.-F. Berret, D.C. Roux, G. Porte, *Proceedings of the IVth European Conference on Rheology*, edited by C. Gallegos (Seville, 1994) pp. 582.
26. G. Porte, J.-F. Berret, J.L. Harden, J. Phys. II France **7**, 459-472 (1997).
27. P. Boltenhagen, Y. Hu, E.F. Matthys, D. Pine, Phys. Rev. Lett. **79**, 2359 (1997).
28. E.K. Wheeler, P. Fischer, G.G. Fuller, J. Non Newtonian Mech. **75**, 193-208 (1998).
29. G. Porte, R. Gomati, O. El Haitamy, J. Applell, J. Marignan, J. Phys. Chem. **90**, 5746-5751 (1986); R. Gomati, J. Applell, P. Bassereau, J. Marignan, G. Porte, J. Phys. Chem. **91**, 6203-6210 (1987).
30. G. Porte, J. Marignan, P. Bassereau, R. May, J. Phys. France **49**, 511-519 (1988); J. Appell, P. Bassereau, J. Marignan, G. Porte, Progr. Colloid Polym. Sci. **81**, 13-18 (1990).
31. G. Porte, J.-F. Berret, in preparation (1998).
32. P. Lindner, R.C. Oberthür, Rev. Phys. Appl. **19**, 759 (1984).
33. D.C. Roux, J.-F. Berret, G. Porte, E. Peuvrel-Disdier, P. Lindner, Macromol. **28**, 1681 (1995).
34. J.-F. Berret, D.C. Roux, J. Rheol. **39**, 725-741 (1995).
35. E. Cappelaere, J.-F. Berret, J.-P. Decruppe, R. Cressely, P. Lindner, Phys. Rev. E **56**, 1869-1878 (1997).
36. J.-P. Decruppe, private communication.
37. M. Deutsch, Phys. Rev. A **44**, 8264 (1991).
38. P. Davidson, D. Petermann, A.M. Levelut, J. Phys. II France **5**, 113 (1995).